

Ferroelectricity in Strain-Free SrTiO₃ Thin Films

H. W. Jang,¹ A. Kumar,² S. Denev,² M. D. Biegalski,³ P. Maksymovych,³ C.W. Bark,¹ C. T. Nelson,⁴ C. M. Folkman,¹ S. H. Baek,¹ N. Balke,³ C. M. Brooks,^{2,5} D.A. Tenne,⁶ D. G. Schlom,⁵ L. Q. Chen,² X. Q. Pan,⁴ S. V. Kalinin,³ V. Gopalan,² and C. B. Eom^{1,*}

¹*Department of Materials Science and Engineering, University of Wisconsin, Madison, WI 53706, USA*

²*Department of Materials Science and Engineering, Pennsylvania State University, PA 16802, USA*

³*Center for Nanophase Materials Sciences, Oak Ridge National Laboratory, Oak Ridge, TN 37831, USA*

⁴*Department of Materials Science and Engineering, University of Michigan, Ann Arbor, MI 48109, USA*

⁵*Department of Materials Science and Engineering, Cornell University, Ithaca, NY 14853, USA*

⁶*Department of Physics, Boise State University, Boise, ID 83725-1570, USA*

Biaxial strain is known to induce ferroelectricity in thin films of nominally non-ferroelectric materials such as SrTiO₃. However, even strain-free SrTiO₃ films and the paraelectric phase of strained films exhibit bulk frequency-dependent polarization hysteresis loops on the nanoscale at room temperature, and stable switchable domains at 50 K. By a direct comparison of the strained and strain-free SrTiO₃ films using dielectric, ferroelectric, Raman, nonlinear optical and nanoscale piezoelectric property measurements, we conclude that SrTiO₃ films and bulk crystals are relaxor ferroelectrics, and the role of strain is to stabilize longer-range correlation of preexisting nanopolar regions, likely originating from minute amounts of unintentional Sr-deficiency in nominally stoichiometric samples. These findings highlight the sensitive role of stoichiometry when exploring strain and epitaxy-induced electronic phenomena in oxide films, heterostructures, and interfaces.

* E-mail: eom@engr.wisc.edu

77.84.Dy, 77.22.Ej, 77.55.+f, 77.65.-j

Pure SrTiO₃ (STO) is a quantum paraelectric material where quantum fluctuations of atomic positions suppress a ferroelectric transition, leading to a stabilized paraelectric state at very low temperature [1,2]. Because the quantum paraelectric state in STO is so close to a ferroelectric state, the material behaves as a so-called incipient ferroelectric [3,4]. Surface ferroelectricity in a few monolayers of SrTiO₃ has been predicted and observed [5–7]. Bulk piezoelectricity and ferroelectricity in the volume of SrTiO₃ can be induced by Ca doping [8], the application of electric field [3,9], mechanical stress [10], and ¹⁸O substitution [11] in the low-temperature regime. It has been demonstrated that tensile-strained commensurate epitaxial STO films can be ferroelectric at room temperature [12,13]. However, a recent study shows that strained STO films on DyScO₃ are not normal ferroelectric but relaxor ferroelectric likely due to Sc doping [14]. Furthermore, STO films grown on (001) STO substrates under low oxygen pressures have been observed to be ferroelectric at room temperature owing to the unusual tetragonality and increased unit cell volume [15]. Therefore, the precise nature of strain-induced ferroelectricity in STO films is still unclear, with variously cited roles of strain, doping, abnormal cell volumes in a range of films deposited on different substrates and under different conditions.

In this Letter, we shed light on the nature of strain-induced ferroelectricity in well-controlled, normal unit cell volume, STO single crystal films. A direct comparison between 1.18%-compressively strained and strain-free STO epitaxial thin films has been performed through temperature-dependent capacitance, ferroelectric polarization, optical Raman and second harmonic generation, and piezoresponse force microscopy (PFM) measurements. Both strained and strain-free films show polarization hysteresis at room temperature; however, the ferroelectricity is unstable without an applied field, and decays away with time within seconds. The decay of PFM signals of the strain-free and strained STO films follows Vogel-Fulcher

behavior indicating that both STO films are relaxor ferroelectrics, by analogy with $\text{Pb}(\text{Mg}_{1/3}\text{Nb}_{2/3})\text{O}_3\text{-PbTiO}_3$ (PMN-PT) films [16]. Raman studies show polar modes present in all SrTiO_3 films as well as in single crystals, and increasing in amplitude in films with intentionally increasing Sr-deficiency. We conclude that the apparent role of strain is to stabilize long-range correlation between nanopolar regions in the volume of the film, likely arising from Sr-deficiency.

(001) STO films were grown on (110) NdGaO_3 (NGO) and (001) STO substrates using pulsed-laser deposition (PLD) with *in-situ* reflection high-energy electron diffraction. The pseudocubic in-plane lattice parameters of the NGO substrate are 3.863 ± 0.0015 Å and 3.854 ± 0.0015 Å. This corresponds to an average biaxial compressive strain of $\sim 1.18\%$ in a fully commensurate STO film on the substrate. We used lattice-matched $\text{Sr}_{0.2}\text{Ca}_{0.8}\text{RuO}_3$ (SCRO) bottom and top electrodes on NGO [17]. On SCRO/NGO substrates, 60 nm thick strained STO films were grown, which were thick enough for electrical measurements. The full width at half maximum (FWHM) of the strained STO films is as small as $0.003\pm 0.0005^\circ$, which is much narrower than that of the bulk STO single crystal. For strain-free STO films on STO with a 50 nm thick SrRuO_3 (SRO) bottom electrode, the volume of the films is measured to be same as that of the substrate, which provides evidence that the PLD-grown STO films are free from excessive point defects as is likely the case in the previous report [15]. The surface of films was atomically smooth with single unit cell height steps measured by atomic force microscopy (AFM).

The enhancement of ferroelectric transition temperature by epitaxial strain can be evaluated by temperature-dependent capacitance measurements as shown in Fig. 1(a). The strain free STO capacitance data are well fit by the Curie–Weiss law, $\varepsilon(T) \propto (T - T_C)^{-1}$ where ε is the dielectric constant, consistent with bulk single crystals. The 60 nm thick strained film on NGO

exhibits maximum capacitances at 120–140 K, well within the theoretically predicted temperature range of 80–230 K [12]. The temperature T_m of the ϵ maximum is shifted to higher values at higher frequencies. This strong dielectric dispersion is evidence leading to a Vogel-Fulcher behavior described by $f = f_0 \exp[-E_a/k_B(T_m - T_f)]$ where f_0 is the attempt frequency, E_a the activation energy, k_B the Boltzmann constant, and T_f the static freezing temperature. $T_m(f)$ of the strained STO is well fit with $T_f = 85$ K, $E_a = 0.081$ eV, and $f_0 = 4.0 \times 10^{12}$ Hz. The E_a and f_0 are reasonable values for typical relaxor behavior [18].

The temperature-dependent polarization of both the strained and strain-free STO films is plotted in Fig. 1(b). Negligible remanent polarization (P_r) is detected in the strain-free film, whereas the strained film displays a ferroelectric polarization-electric field (P - E) hysteresis loop with the P_r of $\sim 9.5 \mu\text{C}/\text{cm}^2$ at 7 K. The gradual decrease of P_r below T_m is different from normal ferroelectrics including BiFeO₃ (BFO) which shows an abrupt drop in polarization at the ferroelectric transition [19]. The ferroelectric transition of the strained STO films can also be evaluated by temperature-dependent optical second harmonic generation (SHG) measurements as shown in Fig. 1(c). For the strained film, no SHG was observed from the NGO substrate or the SCRO bottom electrode. The SHG signal was thus attributed only to the STO film. Compared with a STO single crystal, the strained STO film shows stronger SHG signal at room temperature and a strong temperature dependence. Similar to P_r , the SHG signal decreases gradually with increasing temperature, which is significantly different from normal ferroelectric BaTiO₃ that shows a sharp decrease of SHG signal at the ferroelectric transition temperature [20]. An important thing to note is that finite SHG signal still exists even at room temperature for both the film and bulk single crystal, indicating the presence of nanopolar regions in both [21].

Domain writing/reading or hysteresis loops by PFM are widely used to check whether thin films are ferroelectric [22]. Since PFM signal arises from a ~ 100 nm volume under the tip,

these measurements on our 50 nm thick films are volume responses. Figure 2(a) shows amplitude-contrast PFM image after applying -12 V to $2.5 \times 2.5 \mu\text{m}^2$ area for a strained STO film on NGO at room temperature. The larger piezoresponse signal of the poled region clearly indicates the feasibility of domain writing/reading by PFM even at room temperature well above T_m . For strain-free STO films, there was no signature of poling observed in the slow domain writing and subsequent reading process which typically takes 10–30 minutes each. However, the PFM contrast for the strained STO film gets weaker with time [Fig. 2(a)] and completely disappeared after 10 hours. This suggests that the field induced long-range correlation between preexisting nanopolar regions thermally decays with time in the strained STO film. Autocorrelation maps of these images were calculated following a procedure outlined earlier [23]. The average autocorrelation function versus distance in Fig. 2(b) shows that the correlation length, ξ , under electric fields can extend up to > 1000 nm at room temperature (similar to the size of the written domain pattern), and it collapses to < 100 nm (noise floor) over 10 hours after the removal of the field.

Figure 2(c) shows PFM hysteresis loops with short and long pulse-off duration times for strain-free and strained STO films. The strained film shows significantly enhanced ferroelectric hysteresis loops, but even the strain-free film shows ferroelectric hysteresis loops. With longer pulse-off duration, the loops degrade. Thus, a time-dependent decay of the PFM signal, which is proportional to the net polarization, is observed in both the PFM domain writing/reading and hysteresis loop measurements. To confirm the decay of the PFM signals, we have measured the PFM signal as a function of time after poling at -25 V for both films, as plotted in Fig. 2(d). The strained film shows a larger signal and a much slower decay, whereas the unstrained STO shows a rapid decay of the PFM signal. The lack of PFM signal from a mica sample, for example, implies that the behavior is not due to charge injection or other artifacts from surface interaction.

The gradual decay of the PFM signals has been fit to the power-law decay equation, $P(t) = P_0 t^{-\alpha}$ where P_0 is the magnitude of the initial PFM signal and α the decay exponent. The linear behavior in $\log[P(t)]$ versus $\log[t]$ plots in Fig. 2(e) verifies that the decay of the PFM signals in both STO films on NGO and STO follow the power-law behavior at room temperature, meaning that the decay of the PFM signals is a thermal process. The smaller slope, α , of the strain-free film corresponds to the higher stability of the field-induced local ferroelectricity. We have also measured the PFM signal as a function of time after poling for a typical normal ferroelectric film (BFO) and a typical relaxor ferroelectric film (PMN-PT). The normal ferroelectric BFO film on (001) STO (with a T_C of 830 °C) [24] shows no decay in PFM signal for the measured time period. In contrast, the relaxor PMN-PT film on (001) STO [25] shows decay, and its behavior is analogous to that of the strained STO film. The smaller α and the higher P_0 values in the PMN-PT film is attributed to its higher ferroelectric transition temperature than that of the STO film. These results, as well as the observation of the gradual decay of local contrast (as opposed to the domain-wall driven contraction), suggest that the decay of the PFM signal reflects the relaxor nature of the material. Since the PFM signal is free from polarization relaxation by backswitching due to the depolarization effect [26,27], the P_0 and α values are intrinsic properties. The P_0 value represents the magnitude of the spontaneous polarization of the material and whether the material is a normal ferroelectric or a relaxor is reflected by the α value.

In order to rule out extrinsic effects of surface electrochemistry [28] or charge injection (electret effect) mediated by mobile ions in the ambient atmosphere, we have carried out control PFM measurements under ultra-high vacuum (2×10^{-10} Torr) at 50 K–300 K. The measurements confirm the presence of switchable polarization on the strained film, and very weak ferroelectric hysteresis on the strain-free film, in qualitative agreement with the ambient measurements in Fig.

2. At a low temperature of 50 K, we have been able to pole both STO films [Figs. 3(a) and 3(b)] and the polarization domain patterns were stable on at least 30 min time-scale. The vacuum PFM has confirmed the presence of electric-field induced spontaneous polarization in the strained film, and revealed that the strain-free film also attains such a behavior at low temperatures.

Our experimental results strongly indicate that both strain-free and strained STO films exhibit relaxor behavior at low temperatures. The origin of the relaxor behavior should be nanopolar regions as suggested by Fig. 1(c). Figure 4(a) shows the Raman spectra of five different material systems based on STO. The key result is the appearance of first order Raman scattering by polar modes (TO_2 , LO_3 , TO_4 , and LO_4) in all the film systems. The $SrTiO_3$ single crystal also shows weak signatures of TO_2 and TO_4 modes, which is consistent with the SHG signal and indicates weak polar nature. The polar modes are weak in the nearly stoichiometric MBE film, and are the strongest in the nonstoichiometric ($Sr_{0.9}TiO_{3-x}$) film, which has intentionally introduced large Sr deficiency. The 50 nm thick STO film of this study also exhibit strong polar modes. Nearly identical behavior is observed in the 1 μm thick film. The temperature dependence of the polar modes in the 50 nm thick film is shown in Fig. 4(b). It clearly indicates that the film remains polar up to 350–400K, which is consistent with the optical and PFM observations. Chemical composition analysis by wavelength dispersive x-ray spectroscopy (WDS) on the 1 μm thick STO film indicates that the film has a Sr/Ti ratio of ~ 0.97 , which is stoichiometric within experimental error. These findings indicate that the most likely reason for the ferroelectricity is a small amount of Sr-deficiency in our nominally stoichiometric STO films. Although relaxor ferroelectricity is well known in other materials systems [29–32], an important distinction between STO and other well known relaxor systems is that they involve multiple *A*-site cations by intentional doping, while STO has only Sr on the *A* site with unintentionally present minute amounts of nonstoichiometry (Sr-deficiency).

In conclusion, we demonstrate relaxor ferroelectricity in the volume of strain-free STO films consisting of nanopolar regions with short correlation lengths. The role of strain is, in a sense, similar to an electric field, in that both can stabilize long-range correlation between preexisting nanopolar regions. The PFM results demonstrate that PFM domain writing/reading or hysteresis loops do not provide sufficient evidence for normal ferroelectricity in films, and their time-dependence has to be measured as well. We believe that the power-law exponent, α as well as the time dependence of the correlation length, ξ , as measured from the decay of the PFM signal are good measures to evaluate the nature of ferroelectricity in thin films. There is tremendous interest in SrTiO₃ today such as for 2-D electron gases of LaAlO₃/SrTiO₃, [33] and in strain-induced ferroelectricity [34]. This study highlights the importance of paying attention to relaxor ferroelectricity from minute amounts of non-stoichiometry in even nominally stoichiometric single crystals and unstrained films of STO arising. Finally, we propose that strain-induced relaxor ferroelectricity can exist in other ABO_3 incipient ferroelectrics such as KTaO₃ and CaTiO₃ where the presence of A -site deficiency is probable due to the volatile nature of the A cation, based on a similar mechanism.

The authors gratefully acknowledge the financial support of the NSF through grants ECCS-0708759, DMR-0906443, DMR-0820404, DMR-0602986, DMR-0908718, DMR-0705127 (CBE), the ONR through grant N00014-07-1-0215, and helpful discussion with Thomas Tybell. The research at ORNL's CNMS was sponsored by the Scientific User Facilities Division, Office of BES, and DOE.

References

- [1] K. A. Müller and H. Bukard, Phys. Rev. B **19**, 3593 (1979).
- [2] W. Zhong and D. Vanderbilt, Phys. Rev. B **53**, 5047 (1996).
- [3] J. H. Barrett, Phys. Rev. **86**, 118 (1952).
- [4] J. Hemberger *et al.*, Phys. Rev. B **52**, 13159 (1995).
- [5] N. Bickel, G. Schmidt, K. Heinz, and K. Müller, Phys. Rev. Lett. **62**, 2009 (1989).
- [6] V. Ravikumar, D. Wolf, and V. P. Dravid, Phys. Rev. Lett. **74**, 960 (1995).
- [7] R. Herger *et al.*, Phys. Rev. Lett. **98**, 076102 (2007).
- [8] T. Mitsui and W. B. Westphal, Phys. Rev. **124**, 1354 (1961).
- [9] P. A. Fleury and J. M. Worlock, Phys. Rev. **174**, 613 (1968).
- [10] W. J. Burke and R. J. Pressley, Solid State Commun. **9**, 191 (1971).
- [11] M. Itoh *et al.*, Phys. Rev. Lett. **82**, 3540 (1999).
- [12] J. H. Haeni *et al.*, Nature **430**, 758 (2004).
- [13] M. P. Warusawithana *et al.*, Science **324**, 367 (2009).
- [14] M. D. Biegalski *et al.*, Appl. Phys. Lett. **88**, 192907 (2006).
- [15] Y. S. Kim *et al.*, Appl. Phys. Lett. **91**, 042908 (2007).
- [16] L. E. Cross, Ferroelectrics **76**, 241 (1987).
- [17] C. B. Eom *et al.*, Science **258**, 1766 (1992); D. L. Proffit *et al.*, Appl. Phys. Lett. **93**, 111912 (2008).
- [18] D. Viehland *et al.*, J. Appl. Phys. **68**, 2916(1990).
- [19] S. M. Selbach *et al.*, Adv. Mater. **20**, 3692 (2008).
- [20] K. J. Choi *et al.*, Science **306**, 1005 (2004).
- [21] A. Vasudevarao *et al.*, Phys. Rev. Lett. **97**, 257602 (2006); S. Denev *et al.*, Phys. Rev. Lett. **100**, 257601 (2008).

- [22] A. Gruverman, O. Auciello, and H. Tokumoto, *Annu. Rev. Mater. Sci.* **28**, 101 (1998).
- [23] V. V. Shvartsman and A. L. Kholkin, *J Appl. Phys.* **101**, 064108 (2007).
- [24] H. W. Jang *et al.*, *Phys. Rev. Lett.* **101**, 107602 (2008).
- [25] S. D. Bu *et al.*, *Appl. Phys. Lett.* **79**, 3482 (2001).
- [26] D. J. Kim *et al.*, *Phys. Rev. Lett.* **95**, 237602 (2005).
- [27] D. D. Fong *et al.*, *Phys. Rev. Lett.* **96**, 127601 (2006).
- [28] S. V. Kalinin, A. Rar, and S. Jesse, *IEEE Trans. Ultra. Ferro. Freq. Contr.* **53**, 2226 (2006).
- [29] A. K. Tagantsev *et al.*, *Phys. Rev. B*, **65**, 012104 (2002).
- [30] M. Tyunina *et al.*, *Phys. Rev. B*, **74**, 104112 (2006).
- [31] M. Tyunina *et al.*, *J. Appl. Phys.*, **101**, 084119 (2007).
- [32] S. Glinšek *et al.*, *Appl. Phys. Lett.*, **94**, 172905 (2009).
- [33] A. Ohtomo, D. A. Muller, J. L. Grazul, H. Y. Hwang, *Nature* **419**, 378 (2002).
- [34] J. H. Haeni *et al.* *Nature* **430**, 758 (2004).

Figure Captions:

Figure 1. (a, b) Temperature dependence of (a) dielectric constant and (b) remanent polarization for a 60-nm-thick STO film NGO (strained) and a 100-nm-thick STO film on STO (strain-free). (c) SHG signals for the strained STO film and a STO single crystal.. The SHG vs. temperature of a 100 nm STO film on STO is indistinguishable from the SHG of a (100) STO single crystal. Insets: (a) fits to the Curie-Weiss law and the Vogel-Fulcher law, (b) P - E hysteresis loops of the strained film, and (c) SHG signals for the strained STO film and from a STO single crystal magnified ~ 12 times. The SHG vs. temperature of a 100 nm STO film on STO is indistinguishable from the SHG of a (100) STO single crystal.

Figure 2. (a) Amplitude-contrast PFM images as poled (0 h), after 2 h, and after 10 h for a 50-nm-thick strained STO film on NGO. The length scale is 1 μm . (b) Correlation function, $C(r) = \sum_r I(r + \Delta r)I(r)$, calculated for (a) as a function of distance in the y -direction. The solid lines are fits to $C(r) = \sigma^2 \exp(-(r/\xi)^{2h})$, where (σ, ξ, h) for 0 h, 2 h, and 10 h are respectively, (~ 0.82 , ~ 1044 , ~ 2.25), (~ 0.71 , ~ 1164 , ~ 2.37), and (~ 0.11 , ~ 100 , ~ 0.91). (c) PFM hysteresis loops for 50-nm-thick strain-free and strained STO films. The loops are measured at room temperature in air with a 100 nm biased tip by applying voltage pulses of 40 ms for domain reversal, followed by variable pulse-off periods during which time the PFM signal is measured to avoid electrostatic contributions. (d) Change of PFM signal before and after poling with -25V. (e) PFM signal as a function of time after poling with -25V for BFO, PMN-PT, strained, and strain-free STO films. Solid black lines are fits to the power-law decay.

Figure 3. Vacuum PFM images (left: amplitude-contrast, right: phase-contrast) of polarization domains recorded at 50 K by scanning the tip biased at $\pm 8-10$ V across the surface of the (a) strain-free and (b) strained STO films.

Figure 4. (a) Ultraviolet Raman spectra of a bulk STO single crystal, a near-stoichiometric STO film grown on STO by molecular-beam epitaxy (MBE), an intentionally Sr-deficient film with composition $\text{Sr}_{0.9}\text{TiO}_{3-x}$ grown on STO by MBE, and nominally stoichiometric 50 nm and 1000 nm thick STO films grown on SRO/STO by PLD at 10 K. (b) Temperature-dependent Raman spectra of the 50 nm thick STO/SRO/STO film.

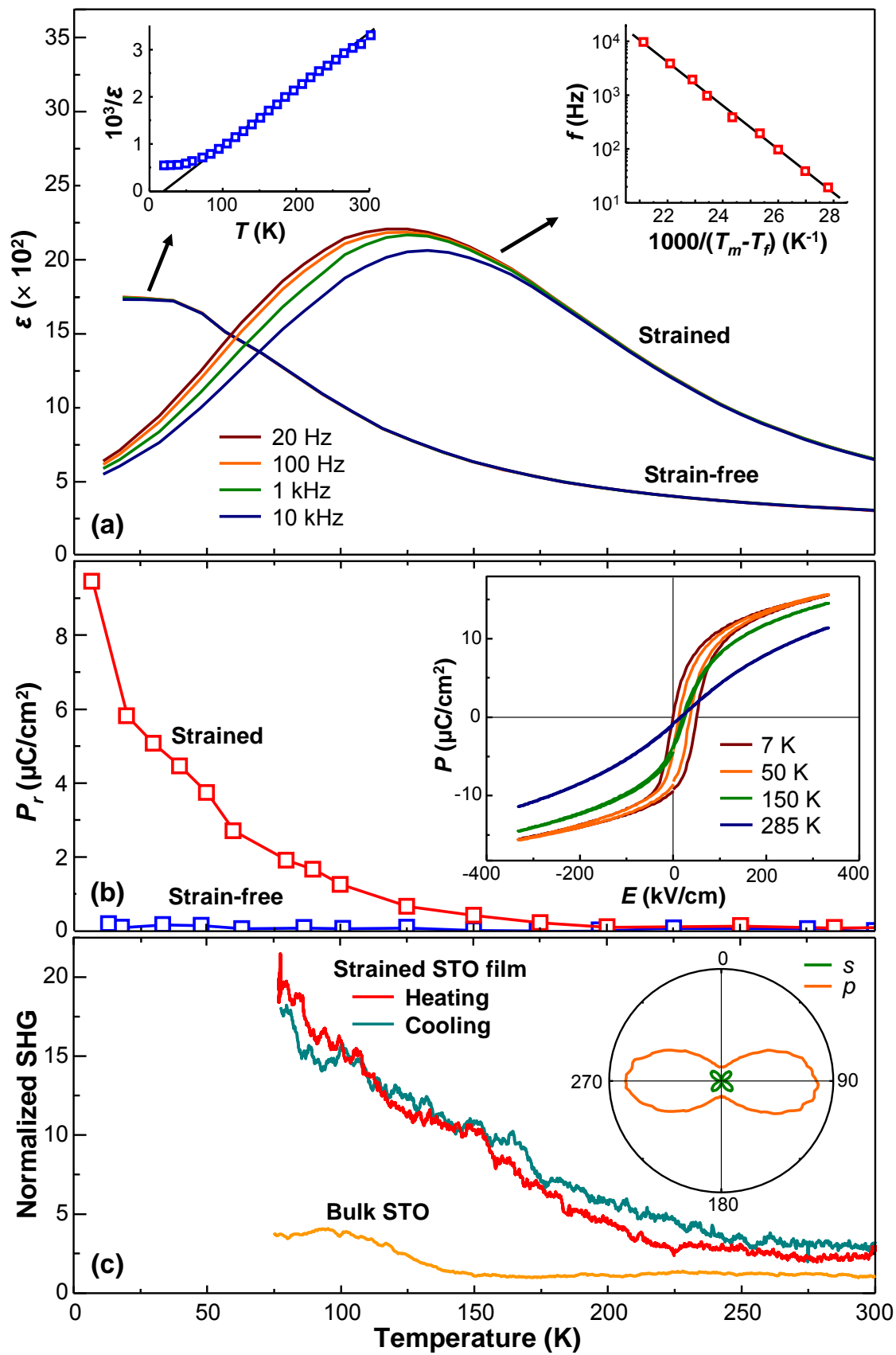


Fig. 1. Jang *et al.*

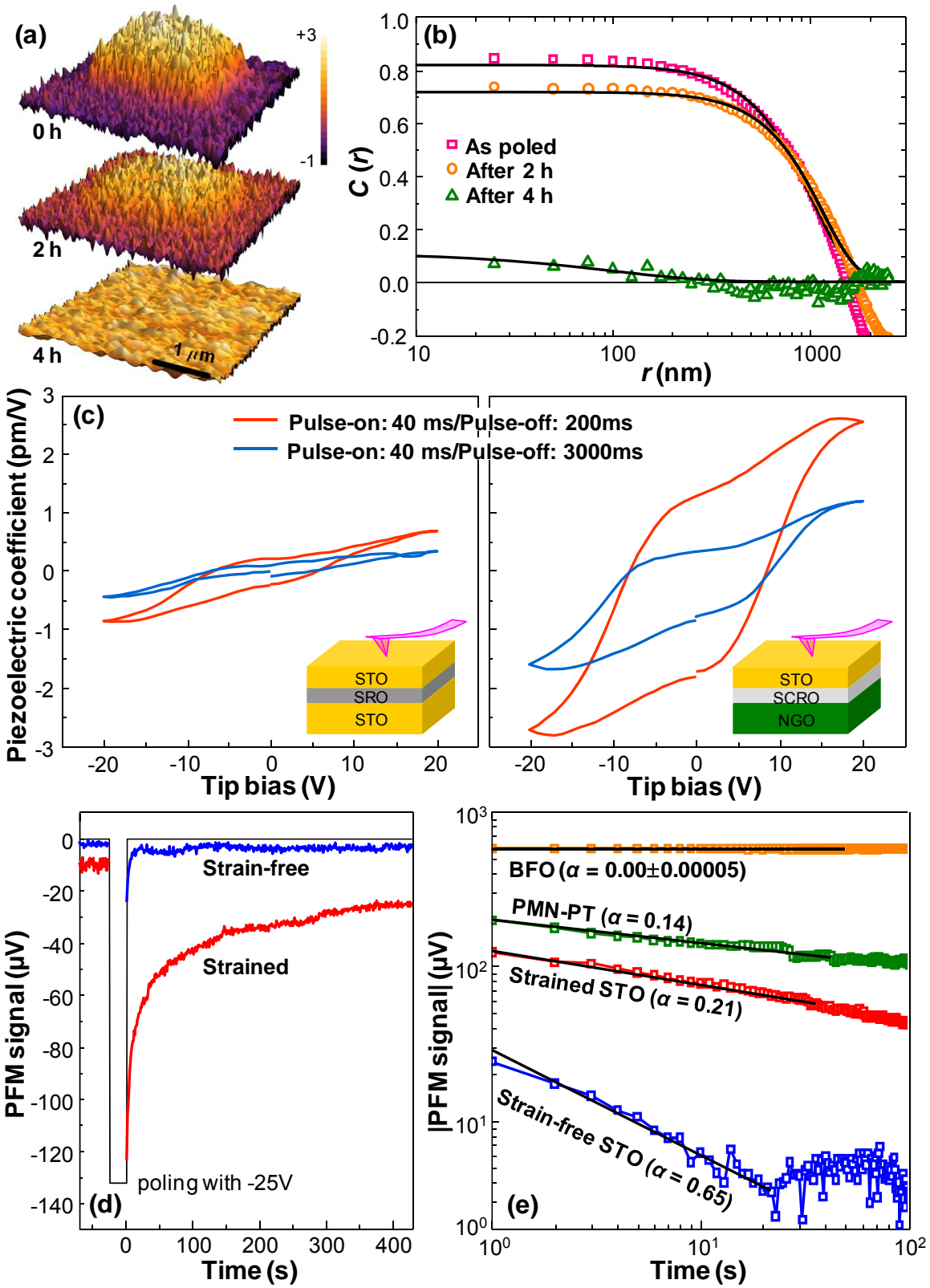


Fig. 2. Jang *et al.*

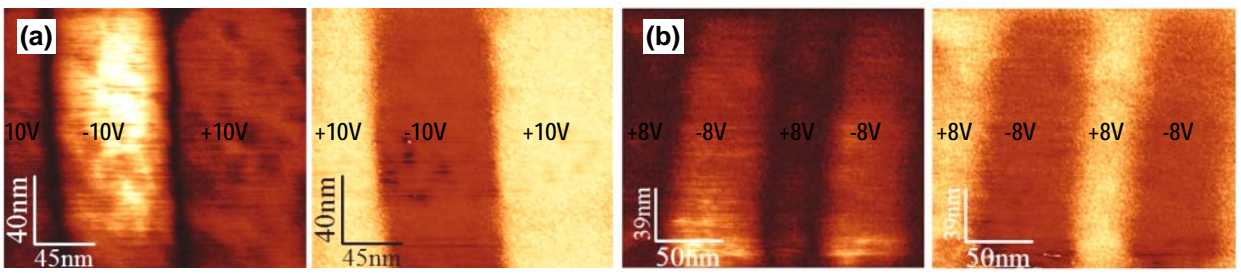


Fig. 3. Jang *et al.*

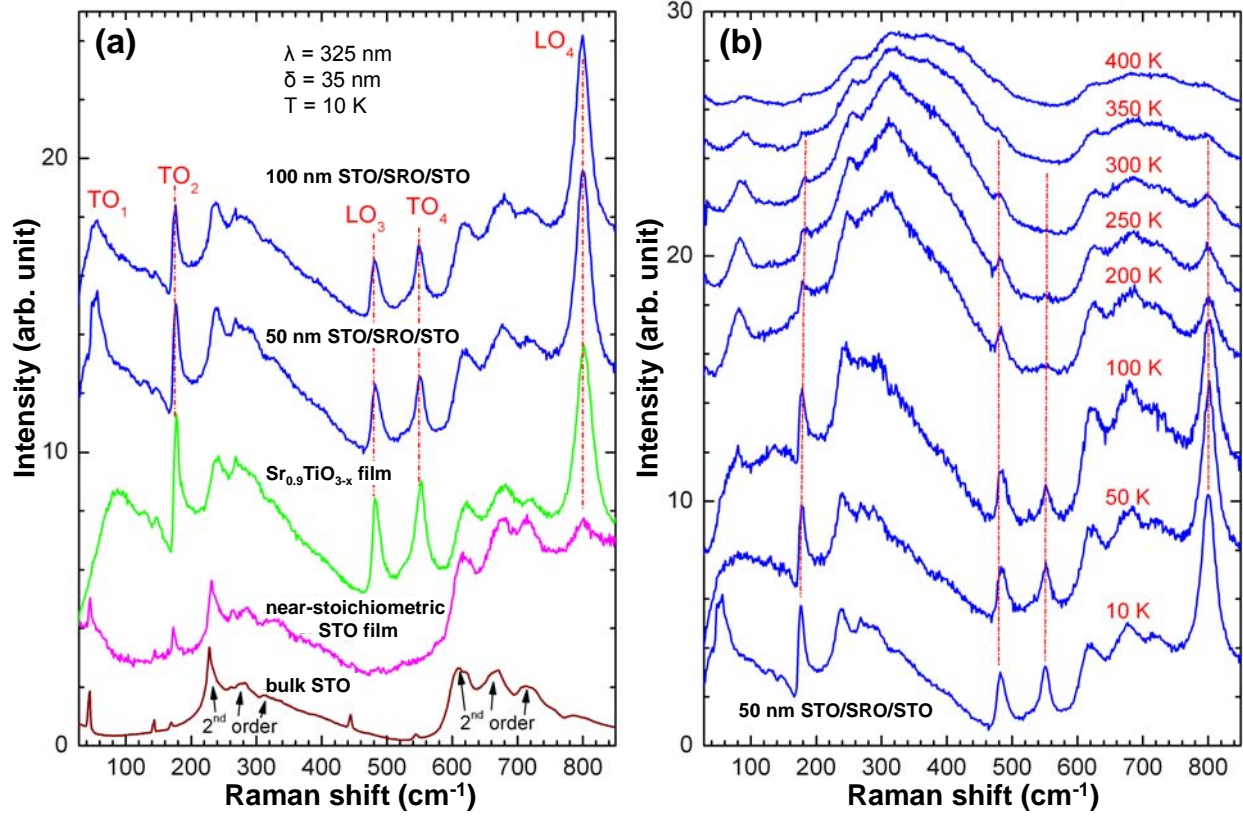


Fig. 4. Jang *et al.*